Brazilian Journal of Geophysics, 43 (2025), 2, 1–27
Brazilian Geophysical Society
ISSN 2764-8044
DOI: 10.22564/brjg.v43i2.2343

IMPACT ASSESSMENT OF INFRASTRUCTURES EXPOSURE TO WEAK MOTION VIBRATIONS IN AREQUIPA, PERU

Jackeline Maria Mamani Sanchez [1], Lady Diana Quispe Torres [1], Ema Milagros Ticona Quispe [1], Cristobal Condori Quispe [1], Yawar Hussain [2], Armando Adolfo Minaya Lizárraga [1], Javier Roberto Ticona Paucara [1], George Sand França [3]

[1]Universidad Nacional de San Agustin de Arequipa, Peru
[2]The University of Texas at Dallas, Richardson, USA
[3]Universidade de São Paulo - USP, Instituto de Astronomia, Geofísica e Ciências Atmosféricas, Brasil

*Corresponding author: jackelin.geo@gmail.com

ABSTRACT. Being an important economic and industrial hub, Arequipa is the second most populous city in Peru, with over one million inhabitants. Within its metropolitan area, high-amplitude vibrations are generated by heavy construction machinery as well as by urban and commercial transportation. These vibrations pose a potential risk of damage to both urban and archaeological infrastructures. To assess possible structural impacts, vibration measurements were collected at significant sites and analyzed according to the DIN 4150-3 standard. Ground vibrations attenuation was evaluated using the Levenberg-Marquardt inversion method. Regression adjustment models were developed, and the analysis of geometric and material damping coefficients was automated with the application of neural network algorithms, in areas with lower data density. The results indicate that vibrations caused by heavy machinery can damage sensitive or residential structures, as the peak particle velocity (PPV) exceeded 20 mm/s in these cases. However, for sources such as vehicular traffic on bridges and railway transport, the PPV only exceeded 10 mm/s. Attenuation analysis revealed that maximum particle velocity decreases with increasing distance from the source, and that the strongest damping occurs in the vertical component. Geometric damping (γ) values ranged from 0.1 to 1.65, and material damping (α) values ranged from 0.001 to 0.03 for the various sources evaluated. In cohesive soils, wave propagation is faster, which reduces tension in the foundations, whereas in sandy-silty soils, slower propagation increases the tension transmitted to the foundations.
This research also aims to lay the foundation for the development of Peruvian regulations framework to assess structural damage caused by anthropogenic vibrations, since there are no existing regulations governing these effects on buildings. This study can help propose guidelines for the city of Arequipa.

Keywords: anthropogenic vibrations; neural networks; attenuation; standard DIN 4150-3; infrastructures

INTRODUCTION

Vibrations generated by either natural (e.g., environment and earthquakes) or anthropogenic sources (traffic, machinery operation, building construction) are major infrastructural risks in populated cities (Yao et al., 2019). Continuous exposure to these vibrations can reduce the strength of buildings, resulting in aging, invisible damage, and collapse under the worst conditions. The close proximity to these vibration sources also has adverse effects on the physical and mental health of residents (Hegde and Venkateswarlu, 2019; Jiang et al., 2020; Niu et al., 2022). The preservation of archeological or other man-made structures, stresses the need for vibrational impact assessment, especially in developing countries (Rodríguez and Bascompta, 2020; Dowding et al., 1996).

Several studies in the literature have documented such impacts. Rodríguez and Bascompta (2020) analyzed poor-quality rock mass exposed to the vibrations generated by machinery such as excavator, ripper, ripper vibrator, hydraulic hammer, bulldozer, and vibrating roller, and proposed several empirical relations to determine maximum particle velocity and ground response intensity at various distances. The peak particle velocity (PPV) represents the maximum intensity of ground vibration and can be used to determine the level of structural safety by comparing it with recommended standards (Athanasopoulos and Pelekis, 2000; Ekanayake et al., 2013). In another study, Burgemeister et al. (2011) used frequency-dependent attenuation and geometric dispersion models to predict maximum vibrations produced by the major construction sources. Furthermore, Khandelwal (2012) compared conventional prediction methods with artificial neural networks for blast-induced ground vibrations, demonstrating that neural networks provide superior accuracy in modeling vibratory response.

Auersch and Said (2010) reported that ground vibrations from various sources attenuate exponentially with distance, with field measurements often exceeding theoretical predictions. Furthermore, Auersch (2010) confirmed that surface wave amplitude attenuation follows a power-law function. This attenuation occurs due to two factors: the expansion of the wavefront (geometric damping) and the dissipation of energy within the soil itself (material damping). Geometric attenuation depends on the type of wave and the shape of the corresponding wavefront (Amick, 1999). Material damping is generally defined as the energy loss due to hysteresis, which is influenced by various parameters, including soil type, moisture content, and temperature (Adam et al., 2011). In more cohesive and rigid soils, the wave propagation velocity is higher, which reduces stresses on foundations and the direct transmission of vibrations to the building. In contrast, in less cohesive soils, such as gravel and sand, the propagation velocity decreases, resulting in increased stress transmitted to the building's foundations (BS 7385-2, 1993). According to Chen et al. (2019), vibration attenuation occurs more rapidly in coarse-grained soils than in fine-grained soils. This can be attributed to the higher porosity and lower moisture content of coarse-grained soils. Another contributing factor is the formation of Love waves (L-waves), which increase shear stress on the surface (Costa, 2011). These findings highlight the importance of studying vibration propagation laws to mitigate their impact on nearby structures and the human population (Chen et al., 2019).

Arequipa is Peru's second-largest city by population, with 1,382,730 inhabitants according to the latest census (INEI, 2018). Founded in 1540 AD, it is commonly known as the "White City" due to the extensive use of sillar in its colonial constructions. This material is also found in various historic buildings in districts such as Cerro Colorado, Cayma, Yanahuara, Socabaya, and Sachaca, where mansions, temples, and plazas serve as important tourist attractions. However, due to their age, these structures are susceptible to structural damage caused by anthropogenic vibrations. These anthropogenic vibrations are generated by vehicles, which, according to Puzzilli et al. (2021), accelerate the degradation of historic structures, increasing their seismic vulnerability and reducing their lifespan. Over the decade 2010–2019, the vehicle fleet in Arequipa has doubled PMUS (2022), a significant factor in the analysis of vertical vibrations on vehicular bridges (Rangel, 2018). Additionally, the railway system in Arequipa generates vibrations in nearby structures and plays a crucial role in transporting minerals and metals, accounting for over 95% of the total cargo moved, this system connects the primary mining centers of southern Peru to the port of Matarani, facilitating international exports (Ositran, 2017). Similarly, the use of heavy machinery in paving projects is mandatory and regulated by national and international standards, including those established by the Ministry of Labor and Employment Promotion (MTPE) and the MTC (2016), which specify operational parameters such as dimensions, geometry, and mass. These vibrating machines generate higher frequencies than explosions, amplifying vibrations in structures (Gasmi et al., 2023).

For controlling anthropogenic vibrations, regulatory standards have been established to set limits before potential structural damage occurs. National and South American standards were analyzed, most of which are used primarily to assess damage to exposed individuals rather than to buildings and structures. International standards such as ÖNORM S9020, BS 7385, USBM, OSMRE, UNE 22, NP-2074-2015, and DIN 4150-3 were also examined. Except for the latter, all of these standards are applied to more intense vibration sources, such as those generated in blasting operations. In this investigation, the DIN 4150-3 standard was applied, which defines three maximum permissible limits. Exceeding these thresholds indicates a potential risk of structural damage to three types of buildings: industrial, residential, and historic.

Vibration analysis is crucial for assessing infrastructure risk in the city. Despite existing studies on the structural analysis of bridges, trains, and machinery in Arequipa, there is a lack of research linking these analyses to structural damage caused by anthropogenic vibration sources. The present study contributes to filling this gap by evaluating the potential structural damage caused by vibrations from machinery such as compaction rollers, vehicular traffic on bridges, and railway operations in the city of Arequipa. This study also seeks to establish the basis for the formulation of a regulatory framework in Peru to evaluate structural damage resulting from anthropogenic vibrations, given the current absence of specific standards addressing these effects on buildings. The findings aim to contribute to the development of technical guidelines applicable to the city of Arequipa. Figure 1a shows the data acquisition points in different districts of the city of Arequipa, with their

respective codes according to the vibration source (details are in Table 1).

The local geology of the city of Arequipa (Figure 1b) includes igneous, sedimentary, and metamorphic units, ranging from the Precambrian to the recent Quaternary. The city's geological diversity is characterized by the presence of alluvial, mudflow, and pyroclastic deposits, resulting from the volcanic origin of the soil (Aguilar and Alva, 1991). The bedrock primarily consists of thick andesitic lava layers, varying in color from dark to light gray, which often weather to reddish or brown hues. Overlying this bedrock, mudflow deposits are prevalent in the districts of Socabaya, Hunter, Cercado, and the western slopes of Misti. Alluvial-fluvial deposits, found in the Arequipa peneplain and on terraces along the Chili River, are composed of gravels, sands, and silts, filling ravines with rounded materials (IGP, 2017). The Cerro Colorado district is influenced by the Chachani Volcanic Complex, characterized by pyroclastic flow deposits and volcanic materials. This area also features ravines that are highly susceptible to lahars during periods of intense rainfall (INGEMMET, 2022). The study area is mainly composed of Quaternary units, with recent deposits of alluvial, volcanic, and pyroclastic origin. The main formations include Holocene alluvial deposits (Qh-al), late Pleistocene pyroclastic flows (Qpl-pi), Neogene volcanic tuffs from the Añashuayco Formation (Nq-añ), units of the Pichu Pichu volcanic complex (Nq-pi), and Lower Cretaceous gabbros (Ki-gb) (INGEMMET, sf). These geological characteristics were used as a reference for the values of the coefficients γ and α, which represent the geometric and material damping coefficients, respectively, and were later calculated using the Levenberg-Marquardt inversion method.

Anthropogenic vibrations generated by heavy machinery, railway transport, and vehicular traffic on bridges in Arequipa, Peru, may exceed the peak particle velocity (PPV) limits specified in DIN 4150-3. These exceedances depend on local soil types, which influence vibration attenuation through geometric (γ) and material (α) damping coefficients. Such propagation governs wave transmission and potential damage to urban and archaeological infrastructures. This study assesses the structural and heritage impacts of these vibrations while modeling ground attenuation using neural networks to estimate damping coefficients. The approach is applied across diverse urban zones in Arequipa to inform risk mitigation strategies.

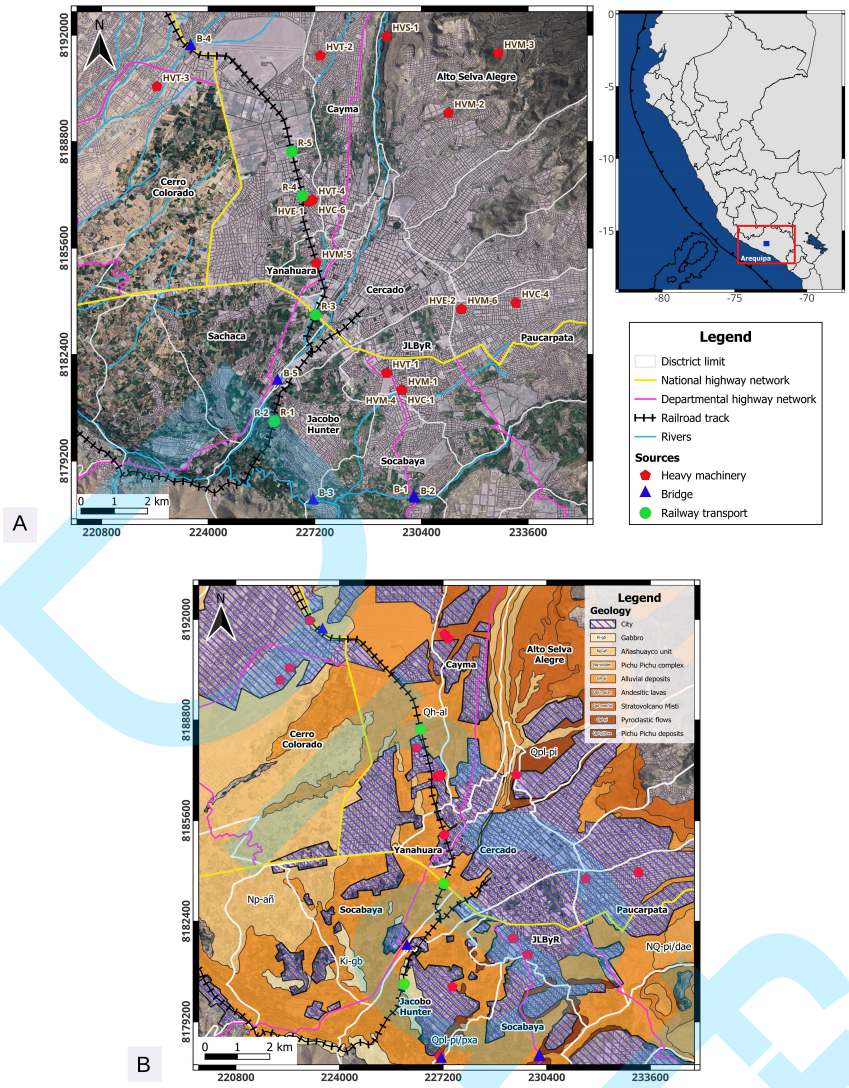

Figure 1: A) Map of the study area showing the distribution of data acquisition points; B) Simplified local geological map of Arequipa (adapted from GeoCatmin platform - INGEMMET). The green circle and red hexagon indicate the locations of vibration recording points.

METHODS

Data

The database used in this study was compiled during 2021 and 2022 and includes records from three main sources of vibration: heavy machinery (road rollers and an excavator with a hydraulic hammer), railway transport, and vehicular traffic on bridges. The possibility of obtaining information from water reservoirs and industrial facilities was also evaluated; however, no significant vibrations were detected in the surrounding structures, so these sources were ruled out. The records were acquired at 2-second intervals, with a duration of 1 minute per measurement. Two Vibracord FX seismometers, provided by the Geophysics Laboratory of the National University of San Agustín de Arequipa (UNSA), were used for data acquisition. This equipment was calibrated following the guidelines established in the international standard DIN 4150-3 (1993), which guarantees the reliability and comparability of the results obtained. These devices interpret electrodynamically induced signals from the coils of high-sensitivity triaxial geophones (operating in a range of 2–250 Hz) and generate peak particle velocity (PPV) measurements in mm/s in their three components: vertical, longitudinal, and transverse. The analysis focused on three sources of anthropogenic vibration: heavy machinery, vehicular traffic on bridges, and

railway transport (Figure 1). The sensors were placed at the base of the structure, oriented toward the vibration source, with some positioned on concrete and others on soil.

Data processing workflow began with a quality check of the recorded information, using an optimal signal-to-noise ratio threshold. In accordance with established standards, vibrations were classified into three groups based on a visual analysis criterion: group A, corresponding to the records with the best response; group B, which includes partially recoverable data but exhibits limitations due to time-shifted points; and group C, comprising records with higher noise levels or deviations from optimal measurement criteria (see Table S2). For the analysis, priority was given to processing group A records, while groups B and C were selectively considered depending on source evaluation and their relevance to the study.

Data corresponding to heavy machinery accounted for 77% of total records, with frequencies ranging from 18 to 90 Hz and particle velocities between 0.5 and 55.70 mm/s. Vibrations generated by traffic on vehicular bridges accounted for 19% of the records, characterized by lower frequencies, ranging from 0.4 to 20 Hz, and velocities between 0.05 and 45.50 mm/s. Finally, railway transport accounted for 4% of the records, with frequencies between 14 and 80 Hz and velocities between 0.09 and 17.43 mm/s. Table 1 summarizes the database used in the study, detailing the sources of vibration, the type of soil, the measurement point code, their respective geographical coordinates, and the total number of records associated with each source.

The most common source of vibrations was heavy machinery. In this study, more than 90% of the machines were road rollers, specifically CAT CS553 models (weighing 10 tons). These machines feature a dynamic drum capable of operating at maximum frequencies of 30 Hz and are mainly used in civil engineering projects during road paving. Additionally, tandem vibratory rollers (weighing 3,500 kg) and an excavator with a hydraulic hammer (weighing 36 tons) were also considered as vibration sources. Vibration signals were recorded at the foundations of buildings (on concrete or soil in various conditions, Figure 2a) and on the roofs of some structures (Figure 2b).

The second major source of vibration was vehicular traffic on concrete bridges. Factors influencing the vibrations included the structural condition of the bridge as well as the weight and speeds of passing vehicles. Data were recorded on the pedestrian sidewalks of the bridges (Figure 2c), approximately 1 meter from the vehicles.

The third vibration source was railway transport, for which data were acquired during the initial field campaign conducted in 2021. During this period, Arequipa remained under a state of emergency related to the COVID-19 pandemic, and recurrent demonstrations by social groups caused interruptions to regular railway operations. Nonetheless, a comprehensive dataset was successfully collected from sites situated within 3 meters of the railway line, characterized by predominantly sandy soil conditions (Figure 2d).

Table 1: Table of vibration data by source and soil type.

Vibration source	Soil type	Point	Coordinates		N° Data (PPV)	N° Data (Attenuation)
			Long.	Lat.		
Heavy machinery	Sand	HVS-1	229353.2	8191966.2	15	1339
	Concrete	HVC-6	227128.1	8187053.1	193	
		HVC-1	229804.8	8181342.5		
		HVC-2	227347.4	8191138.1		
		HVC-3	227347.4	8191138.3		
		HVC-4	233232.1	8183953.3		
		HVC-5	227007.4	8186998.0		
		HVE-1	227050.5	8187014.3	96	
		HVE-2	231593.2	8183763.3		
	Compact soil	HVT-1	229353.2	8181844.4	157	
		HVT-2	227362.5	8191387.3		
		HVT-3	222462.2	8190456.6		
		HVT-4	227128.1	8187053.1		
	Medium compact soil	HVM-1	229817.4	8181329.1	102	
		HVM-2	231212.8	8189661.1		
		HVM-3	232707.3	8191453.6		
		HVM-4	229801.4	8181303.8		
		HVM-5	227240.1	8181515.8		
		HVM-6	231602.9	8183765.2		
Bridge	Concrete	B-1	230173.4	8178091.4	136	1230
		B-2	230195.2	8178041.7		
		B-3	227144.0	8177985.0		
		B-4	223473.0	8191638.0		
		B-5	226081.0	8181538.0		
Railway train	Sand	R-1	225990.3	8180483.0	33	224
		R-2	225984.3	8180389.1		
		R-3	227218.0	8183595.3		
		R-4	226827.0	8187170.0		
		R-5	226511.8	8188505.1		

ANALYSIS OF THE IMPACT OF VIBRATIONS ON STRUCTURES

The Vibration Meter software was used to analyze the vibration records, enabling the visualization of readings obtained by the Vibracord FX equipment (Del Castillo Martinez, 2012). The data were statistically processed in the frequency domain to determine 50% of the energy spectrum. This method minimizes the dispersion typically observed in frequency spectra, allowing for the analysis of the entire dataset to identify wave records with PPV values. Figures 3a, 3b, and 3c show the vibration velocity records induced by a road roller, rail traffic, and vehicular traffic on a bridge, respectively. The maximum velocity values are recorded when the excitation source is at the shortest distance from the seismograph, corresponding to 1.5 m for heavy machinery and between 1.5 and 2 m for sources associated with rail and vehicular traffic.

Table 2 presents the predominant frequencies and PPV values established by the German Standards DIN 4150-3. For the analysis, three frequency intervals were adopted: >10 Hz, 10–50 Hz, and 50–100 Hz.

ANALYSIS OF VIBRATION ATTENUATION

The decrease in wave amplitude with distance from the source is due to two main factors: geometric spreading and material damping. Their combined effect can be described by the relationship proposed by Attewell and Farmer (1973a):

$$v_{\max} = v_0 \left(\frac{r_0}{r}\right)^{\gamma} e^{\alpha(r_0 - r)} \tag{1}$$

Equation (1) describes the level of attenuation of the maximum velocity, also referred to as peak particle

Figure 2: Photographs showing data acquisition along different sources: A) Compactor roller; B) Similar to scenario A, but with sensors installed on the roof of a two-story house in the district of Paucarpata; C) Vehicular traffic on bridges in the district of Socabaya; D) Railway transport near residential areas.

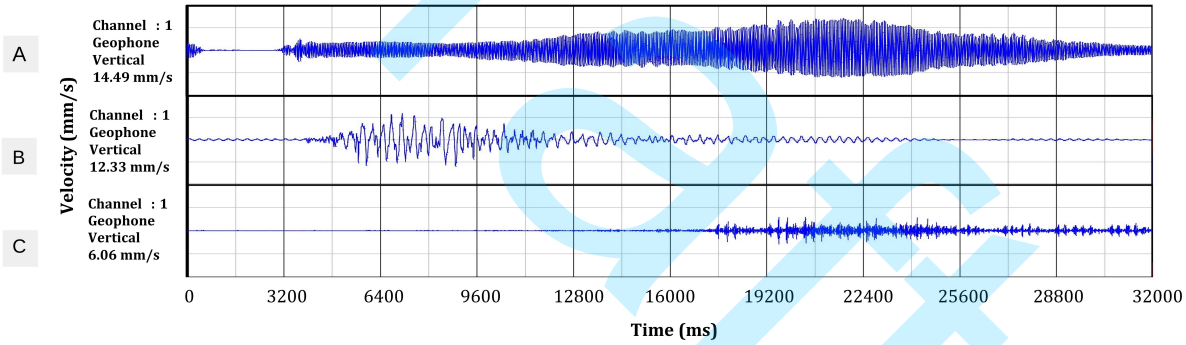

Figure 3: Vibration amplitude variation recorded by two geophones. A) Road roller; B) Vehicular traffic on bridges; C) Railway transport.

Table 2: Vibration control limits established by the German Standards DIN 4150-3 (DIN 4150, 1999).

Type of structure	**Vibration thresholds for structural damage, PPV (mm/s)**			
	Short term			**Long term**
	At foundation	**Uppermost floor**		**Uppermost floor**
	0 to 10 Hz	**10 to 50 Hz**	**50 to 100 Hz**	**All frequencies**
Commercial/industrial	20	20 to 40	40 to 50	10
Residential	5	5 to 15	15 to 20	5
Sensitive/historic	3	3 to 8	8 to 10	2.5

velocity (PPV), according to Rodríguez and Bascompta (2020), representing the product of a hyperbolic and an exponential function. In this formulation, $v_{\max}$ (mm/s) represents the PPV at a distance r from the source, assuming that the initial velocity v_0 (mm/s) at an initial distance r_0 (m) is known. The coefficient γ (dimensionless) is an empirical parameter that represents the geometric damping coefficient, while α (m^{-1}) represents the material damping coefficient. For the analysis, this formulation was applied to predict the

behavior of the maximum velocities as a function of distance, using the initial values of velocity and the position of the machinery, as well as the surface geological characteristics of the recording environment. These characteristics were used to determine the coefficients γ and α. These coefficients were incorporated into the regression adjustment model using the multidimensional nonlinear least squares algorithm with the generalized Levenberg-Marquardt inversion method. The resulting constraints for γ were between (0.1- 1.65), and for α they ranged from (0.001- 0.03) for the objective function.

Levenberg-Marquardt Method

The Levenberg-Marquardt method was used because it incorporates a technique to address the issue of matrix singularity in $J^T(x^{(k)})J(x^{(k)})$ and is an effective algorithm for handling small residuals. In this case, the update is given by:

$$\left[J^T\left(x^{(k)}\right)J\left(x^{(k)}\right)+S\left(x^{(k)}\right)+\mu^{(k)}I\right]\delta^{(x)}=-J^T\left(x^{(k)}\right)f\left(x^{(k)}\right) \tag{2}$$

Where J represents the jacobian matrix and S a necessary condition, x is the real vector of variables, f the function to evaluate, and $x^{(k)}$ a sequence of points, where the index k indicates the number of the current iteration. A strategy to select $\mu^{(k)}$ (2) is shown in Appendix Figure A1 along with a LineSearch implementation scheme (Saucedo, 2014).

The Levenberg-Marquardt (LM) curve fitting method is used to solve nonlinear least squares problems and combines the gradient descent and Gauss-Newton (GN) methods. It addresses the confidence region sub-problem proposed for a given data set by solving the least squares system that involves the Jacobian matrix. This is achieved through the functions "gsl_nls" "gsl_multifit_nlinear" and "gsl_multilarge_nlinear" which are implemented in the RStudio programming environment (Coleman and Verma, 2001).

ARTIFICIAL NEURAL NETWORKS

Artificial neural networks (ANNs) are widely employed across various applications and are particularly popular in system modeling due to their efficiency in adaptation and learning through pattern recognition (Mia and Dhar, 2016). Keras (Chollet et al., 2015) and TensorFlow (Abadi et al., 2016) were selected for implementation owing to their robust support for regression tasks, as evidenced in geophysical applications (Goodfellow et al., 2016).

The methodology was structured into five phases. In the first phase, an experimental dataset comprising distances (meters) and peak particle velocities (PPV, in mm/s) was compiled for ANN training. In the second phase, a set of distance values within the experimental range was selected to predict PPV in inaccessible areas—attributable to state-mandated lockdowns, paving disruptions, strikes, or blockades—thereby avoiding any extrapolation beyond observed maxima and ensuring reliable predictions. In the third phase, the ANN architecture was configured with an input layer of 32 neurons (to capture complex attenuation patterns), a hidden layer of 16 neurons (reducing dimensionality and optimizing computational efficiency), and an output layer consisting of a single neuron with linear activation for PPV regression. This 32-16-1 configuration was derived from established practices for small datasets, balancing expressiveness against the risk of overfitting (Goodfellow et al., 2016; Bishop, 1995); additionally, ReLU activation was applied in the hidden layers to effectively manage inherent nonlinearities in limited data (Glorot et al., 2011). In the fourth phase, the model was trained using the Adam optimizer Kingma and Ba (2014) with a learning rate of 0.1, selected after evaluating preliminary values (0.001, 0.01 and 0.1), which demonstrated minimization of validation RMSE with efficient convergence. The data were split into 70% for training, 20% for validation, and 10% for testing, tailored to the reduced dataset size (Hastie et al., 2009). The training process spanned 1000 epochs, achieving convergence without notable overfitting, owing to the simplicity of the univariate regression and the moderate architecture (Goodfellow et al., 2016). Post-training validation confirmed low RMSE values. Figure 4 shows the applied neural network scheme, which indicates the input variable "r1" as a function of distance, the hidden layers, and the output "PPV" as a function of peak particle velocity.

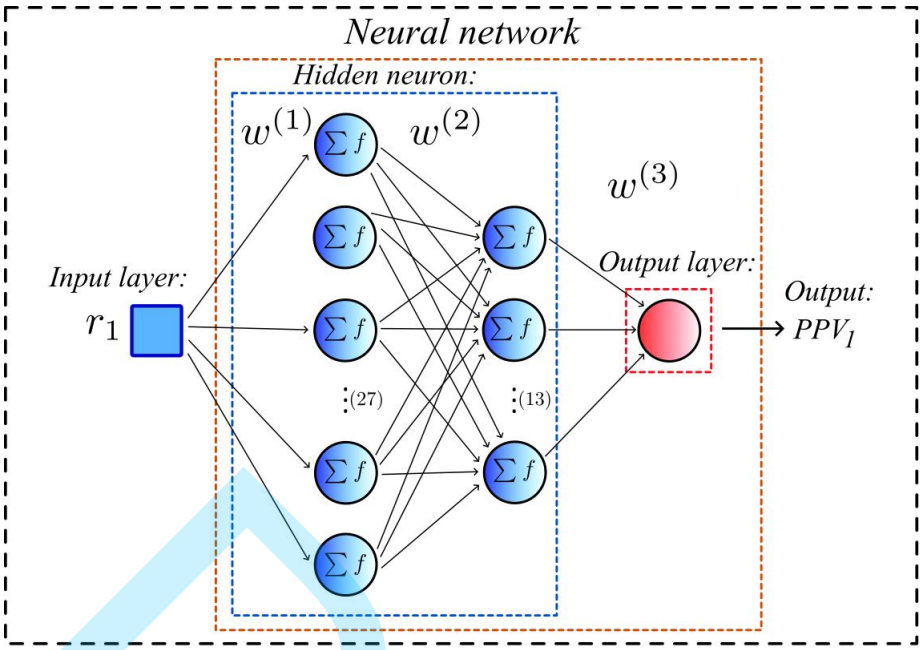

Figure 4: Scheme of an Artificial Neural Network (ANN) used in this study.

RESULTS

VIBRATION SOURCE

The measurements correspond to the base of the dwellings; in concrete foundations (Figure 5a) and compacted soils (Figure 5b), the propagation of vibrations generates a significant impact on buildings close to sources of anthropogenic vibration. Maximum peak particle velocity (PPV) values exceeding 40 and 50 mm/s were recorded, with frequencies predominantly in the range of 20 to 60 Hz (vibration frequencies of the compactor roller). These levels exceed the three thresholds established by DIN 4150-3, applicable to sensitive and residential buildings, indicating a potential structural risk. Vibrations of this magnitude can cause cracks to appear, especially when heavy machinery operates in the vicinity of sensitive or historically valuable buildings, structures that currently predominate in the historic center of Arequipa. In contrast, in loose soils (Figure 5c), the vibration waves are considerably attenuated, with PPV values below 10 mm/s, with frequencies mainly between 30 and 40 Hz. A similar pattern is observed in the upper levels of the buildings, where the maximum peak particle velocity (PPV) recorded reaches 40 mm/s, with predominant frequencies around 20 Hz, values due to the resonance of the structure acting as a dynamic filter (Figure 5d). In this scenario, PPV levels also exceed the three limits established by DIN 4150-3 for sensitive, residential, and industrial buildings.

In the vibration record obtained at the 85-meter-long Mansion Fundador bridge, a maximum peak particle velocity (PPV) value of 30 mm/s was recorded, with predominant frequencies below 20 Hz (Figure 6a). Meanwhile, on the 115-meter-long Virgen de Los Remedios Bridge, the maximum PPV reached 45 mm/s, with predominant frequencies below 15 Hz (Figure 6b). In both cases, the vibration levels exceed the three limits established by DIN 4150-3, and there is a marked pattern in the vertical component (V), where the vibrations have the highest PPV values. This behavior suggests a possible amplification due to resonance, caused when the excitation frequency induced by vehicle traffic approaches one of the natural frequencies of the structure. In the records of vibrations caused by railway transport, a maximum peak particle velocity (PPV) value of 18 mm/s was recorded, with predominant frequencies between 30 and 60 Hz, due to the impact of the load carried by trains, which can exceed 20 tons (Figure 6c). These vibration levels exceed two of the three limits established by DIN 4150-3 for residential structures and sensitive or historically valuable buildings located in proximity to the railway line. The degree of impact of these vibrations varies depending on various factors, such as train speed, type of load carried, soil characteristics, and the structural response of adjacent buildings.

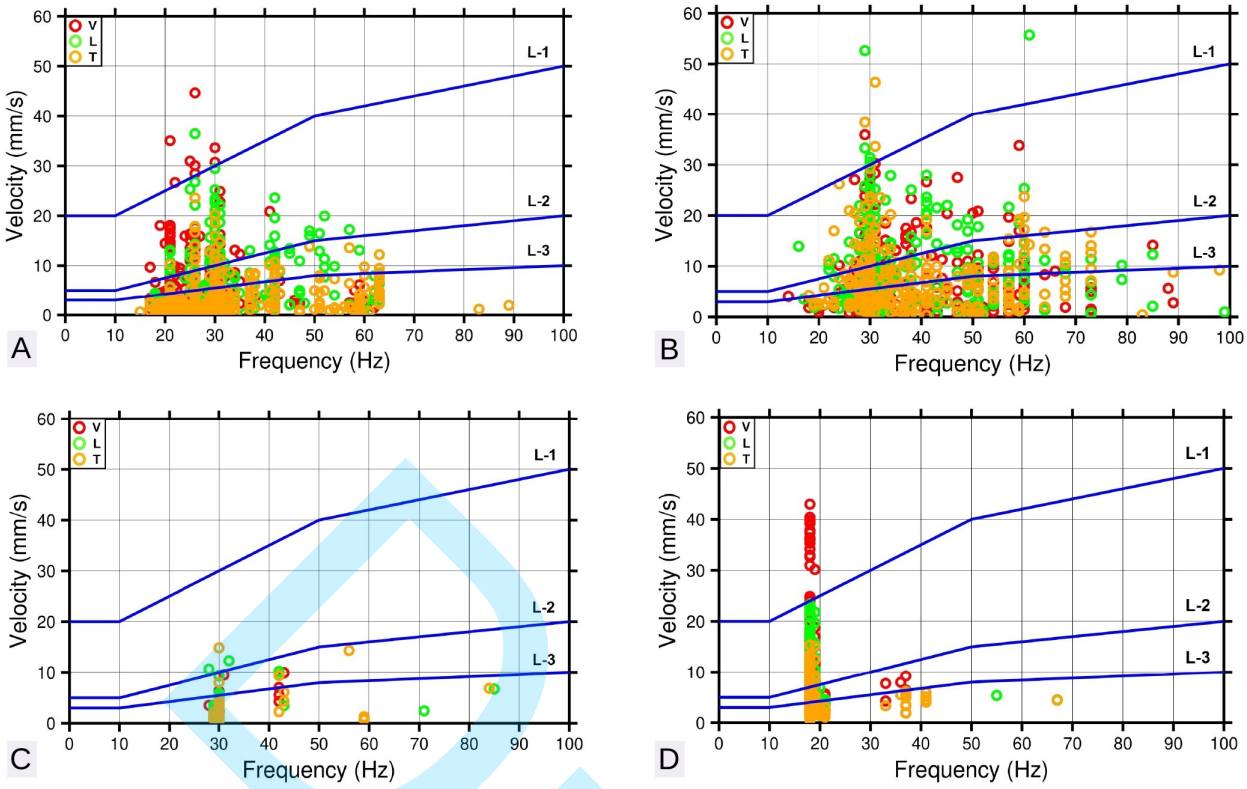

Figure 5: Result of the impact of vibrations generated by the compactor roller, represented within the limits established by the DIN 4150-3 standard (blue lines L-1, L-2 L-3): A) Buildings with cement foundations; B) Buildings with compacted soil foundations; C) Buildings with loose soil foundations; D) Upper floors of buildings.

VIBRATION ATTENUATION AND SITE EFFECTS

The application of neural network algorithms automated the analysis of geometric and material damping coefficient. Figures 7a to 7d represent the PPV values obtained from the compaction roller during paving works in the sectors of Asociación Peruarbo, Avenida Inglaterra, Avenida Cementerio, and Asociación Cesar Vallejo, located in the districts of José Luis Bustamante and Rivero, and Cerro Colorado, respectively. Figure 7e corresponds to the PPV values recorded by an excavator with a hydraulic hammer during civil works in the sector located in Asociación José Luis Bustamante and Rivero (JBR), Cerro Colorado. The field data were compared with those calculated through ANN training, showing root-mean-square (RMSE) values ranging from <0.01 – 0.04>, demonstrating a high degree of correlation between the compared data.

Figures 8a to 8d show the PPV values obtained from vehicular traffic on the following bridges: Añashuayco, Mansión del Fundador, Tingo, and Socabaya, located in the districts of Cerro Colorado, Hunter, and Socabaya, respectively. The field data were compared with values calculated through the training of artificial neural networks, with root-mean-square-error (RMSE) results ranging between <0.003 – 0.03>, demonstrating a high degree of correlation between the compared datasets. The lower data density observed in Figures 8a and 8c, as well as the dispersion seen in Figures 8b and 8d, can be attributed to various factors associated with vehicular traffic on the bridges, such as variations in vehicle speed, vehicle weight and type, load capacity, and the possible presence of overlapping vibrations generated by multiple vehicles crossing simultaneously.

Figure 8e shows the PPV values obtained from railway transport along the route from the district of Cerro Colorado to Sachaca. The field data were compared with values calculated using the trained neural networks, yielding an RMSE value of 0.01, demonstrating a high degree of correlation.

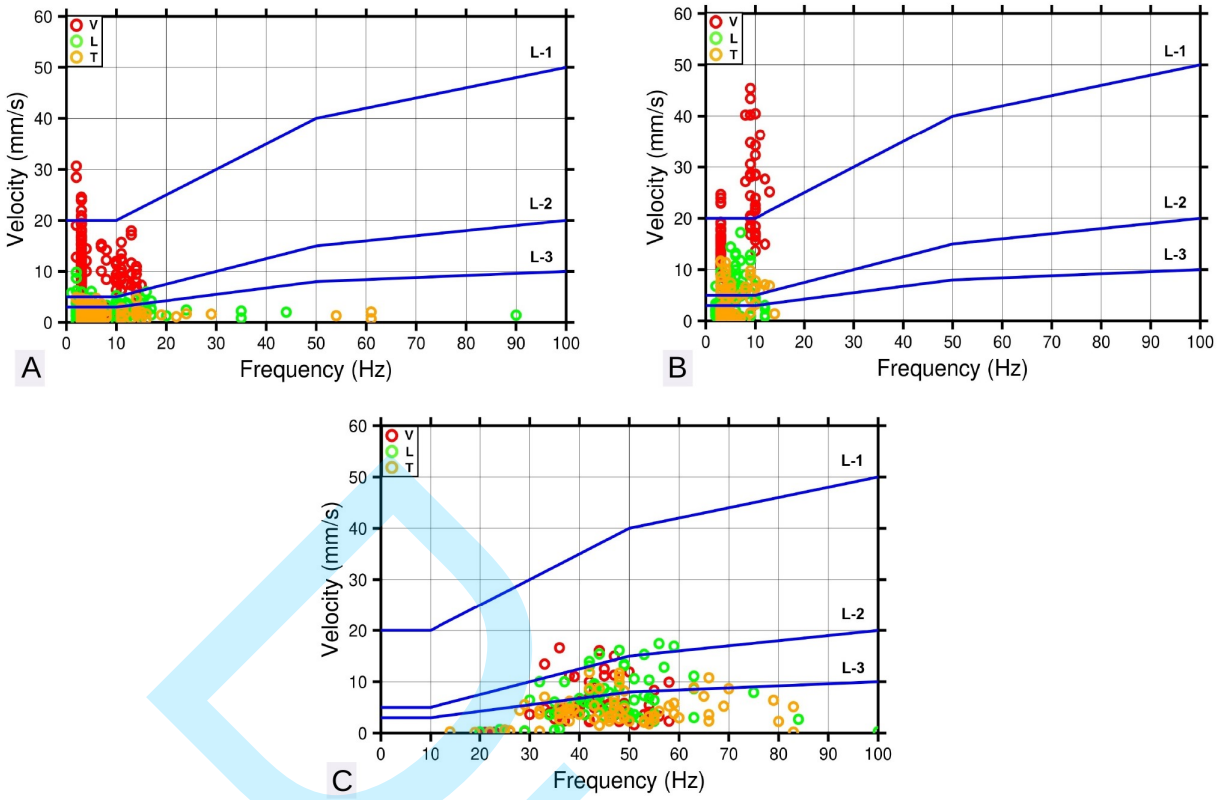

Figure 6: Result of the impact of vibrations generated by the vehicular traffic on bridges, represented within the limits established by the DIN 4150-3 standards (blue lines): A) Mansión del Fundador Bridge; B) Virgen de Los Remedios Bridge; C) Railway transport.

GEOMETRIC AND MATERIAL DAMPING COEFFICIENTS

The values for the coefficients γ and α are provided in Table 3. These values were compared to those reported by various authors to establish a permitted minimum and maximum range, as detailed in Appendix Table S1. Additionally, the greatest vibration damping results occur in the vertical component, as this type of source produces a significantly higher proportion of the vector velocity in this direction. Furthermore, in the near field of the vibration source, the vertical component dominates (Pistrol et al., 2013). For this reason, the results are based on the vertical component. For further details on the results in the other components, refer to Appendix Figures S2 to S4.

ATTENUATION GENERATED BY HEAVY MACHINERY

The theoretical regression model for predicting seismic vibration records from a large drum compactor (road rollers) in the area corresponding to the Asociación Cesar Vallejo, located in the Cerro Colorado district, converges to a solution with $\alpha = 0.03$ and $\gamma = 0.88$, in an arrangement perpendicular to the source path. Another area, Avenida Cementerio in the José Luis Bustamante y Rivero district, where the vibration was generated by a small drum compactor roller (tandem vibratory rollers), converges to a solution with $\alpha = 0.03$ and $\gamma = 1.06$, also in a perpendicular arrangement to the source path. Figures 9a and 9b show solutions that yield curves based on the equation calculated with 95% confidence and prediction limits. For the prediction of seismic vibration records generated by an excavator with a hydraulic hammer in the Asociación José Luis Bustamante y Rivero, also in the Cerro Colorado district, the theoretical regression model converges to a solution with $\alpha = 0.01$ and $\gamma = 0.5$, in an arrangement perpendicular to the source path. This solution produces a curve based on the equation calculated with 95% confidence and prediction limits (Figure 9c).

The vibratory behavior generated by the compaction roller in the two aforementioned areas shows that, for the area corresponding to the Asociación Cesar Vallejo, the attenuation is approximately 31 mm/s at a maximum recording distance of 12 meters. In the case of Avenida Cementerio, the attenuation is approximately 29 mm/s at a maximum recording distance of 10 meters. For the vibratory behavior generated by an excavator with a hydraulic hammer in the same area, the attenuation is around 3.5 mm/s at a maximum recording distance of 13 meters. The results obtained from the Asociación Cesar Vallejo sector show faster attenuation,

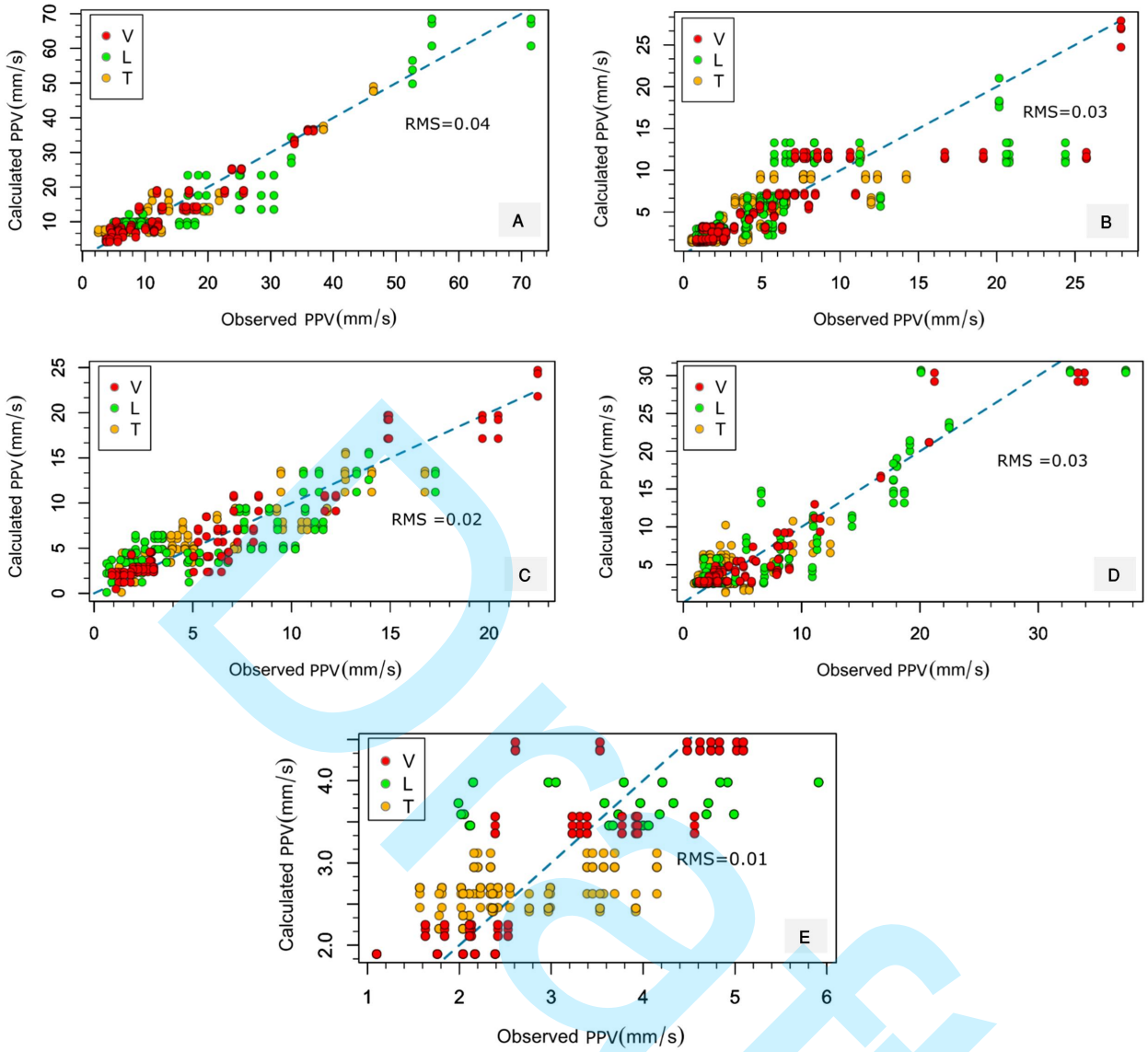

Figure 7: Comparison of data obtained and calculated by artificial neural networks for heavy machinery: A) Asociación Peruarbo; B) Avenida Inglaterra; C) Avenida Cementerio; D) Asociación Cesar Vallejo; E) Asociación José Luis Bustamante and Rivero. The blue dashed line represents the line of agreement between the observed and calculated PPV values. The RMSE value obtained suggests a highly accurate model.

which correlates with the data acquisition area. The coefficients suggest that the material consists of a concrete slab that is granular and compact, with greater porosity and low moisture content. This results in a higher wave propagation velocity, which reduces stresses in the foundations and the direct transmission to the structure. In other words, waves with higher velocities induce less vibration in the foundations. On the other hand, in Avenida Cementerio and the Asociación José Luis Bustamante y Rivero, the decay curve is more gradual, which is associated with a silty-sandy geology. This indicates less cohesive soils, where wave propagation velocity is lower, resulting in higher stress transmission to the foundation.

ATTENUATION GENERATED BY VEHICULAR TRAFFIC ON BRIDGES

The theoretical regression model for predicting seismic vibration records generated by vehicular traffic on bridges in the area corresponding to Mansión del Fundador, Jacobo Hunter district, converges to a solution with $\alpha = 0.02$ and $\gamma = 0.7$. Figure 10 shows that the solution yields a curve based on the equation, calculated with 95% confidence and prediction limits. The vibration behavior generated by vehicular traffic on bridges in the aforementioned area indicates that the attenuation is approximately 27 mm/s at a maximum recording

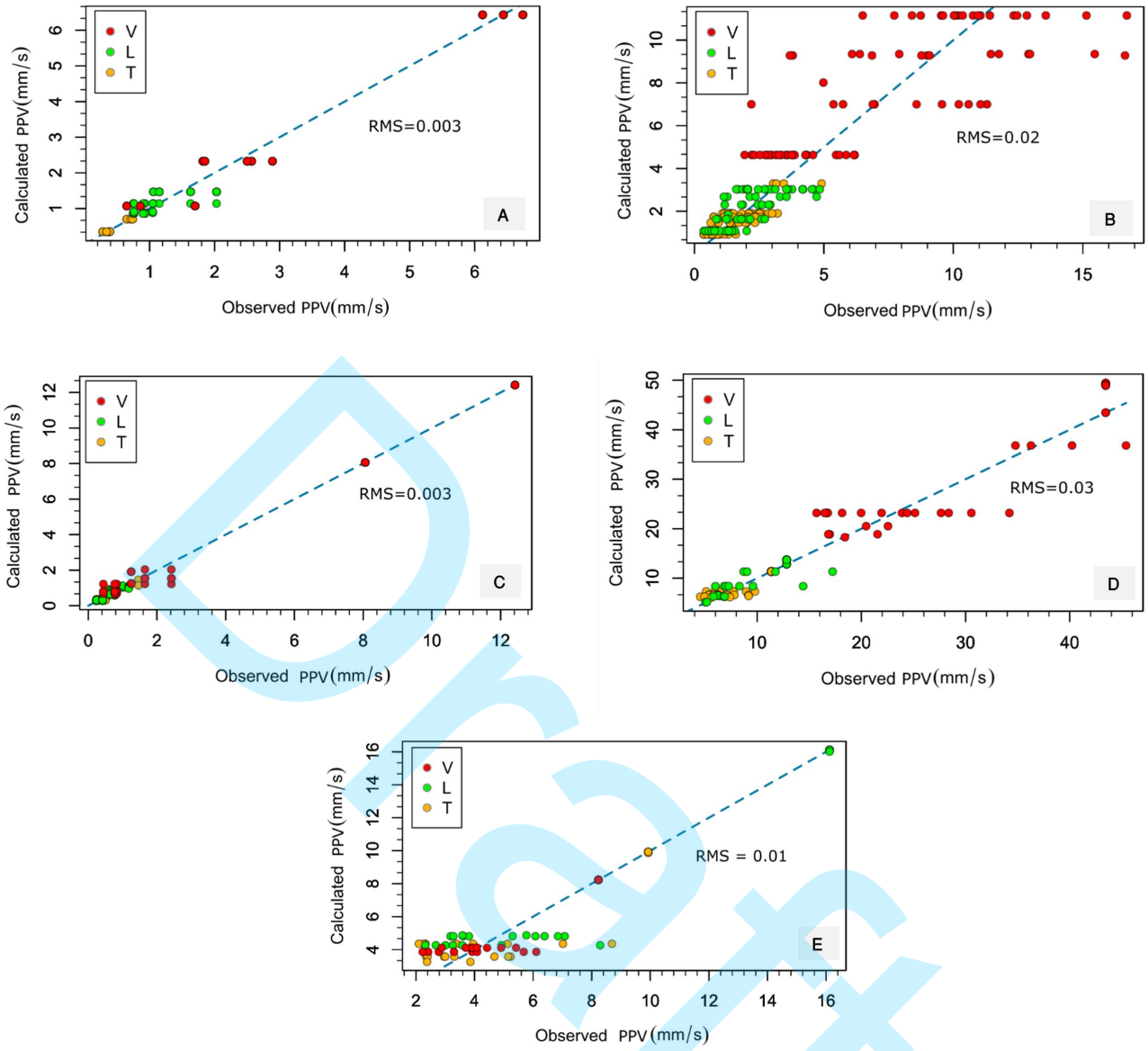

Figure 8: Comparison of the data obtained and calculated using artificial neural networks for vehicular traffic on bridges: A) Añashuayco Bridge, B) Mansión del Fundador Bridge, C) Tingo Bridge, D) Socabaya Bridge; and for railway transport: E) Railway transport records on the route from the district of Cerro Colorado to Sachaca. The blue dashed line represents the line of agreement between the observed and calculated PPV values. The RMSE value obtained suggests a highly accurate model.

distance of 6 meters. The results obtained at the Mansión del Fundador Bridge show faster attenuation, which correlates with the data acquisition area. The coefficients suggest the material consists of a concrete slab that is granular and compact, with greater porosity and low moisture content. This leads to a higher wave propagation velocity, which reduces the stresses on the foundations and minimizes direct transmission to the structure. In other words, waves with higher velocities induce less vibration in the foundations.

ATTENUATION GENERATED BY RAILWAY TRANSPORT

The theoretical regression model for predicting seismic vibration records generated by railway transit along the route from the district of Cerro Colorado to Sachaca converges to a solution with $\alpha = 0.01$ and $\gamma = 0.6$. Figure 11 shows that the solution produces a curve based on the equation, calculated with 95% confidence and prediction limits.

Table 3: Values of α and γ for different sources

Source	Site	Soil type	Distance (m)	α (m^{-1})			γ (m^{-1})		
				V	L	T	V	L	T
Vehicular traffic	Añashuayco	Volcanic tuffs	4	0.02	0.02	0.02	0.8	0.82	0.4
	Mansión del Fundador	Alluvial deposits and gabbros	6	0.02	0.02	0.01	0.7	0.8	0.6
	Socabaya	Pichu Pichu volcanic complex	7	0.01	0.01	0.02	0.6	0.6	0.33
	Tingo	Alluvial deposits	4.5	0.02	0.02	0.02	1.65	1.7	1
Railway transport	Cerro Colorado and Sachaca	Alluvial deposits and pyroclastic flows.	6	0.01	0.05	0.02	1.21	0.84	0.84
	Av. Inglaterra	Pyroclastic flows and andesitic deposits	9	0.03	0.03	0.03	0.9	0.8	0.7
Heavy machinery	Asoc. Cesar Vallejo	Alluvial deposits and volcanic tuffs	12	0.03	0.03	0.03	0.8	0.8	0.7
	Asoc. Peruarbo	Volcanic tuffs	7	0.03	0.03	0.03	0.67	0.73	0.68
	Av. Cementerio	Alluvial deposits and pyroclastic flows.	10	0.02	0.02	0.02	0.65	0.6	0.7
	Asoc. JBR	Pyroclastic flows and units of the Pichu Pichu volcanic complex	13	0.01	0.01	0.01	0.5	0.5	0.1

The vibratory behavior generated by railway transport in the aforementioned area shows an attenuation of approximately 10 mm/s at a maximum recording distance of 6 meters. The results obtained from railway transport along the route from the district of Cerro Colorado to Sachaca indicate a gradual decay curve, which is associated with silty-sandy geology. This suggests the presence of less cohesive soils with lower porosity and higher moisture content, where the propagation velocity decreases, thereby increasing the stress transmitted to the foundation.

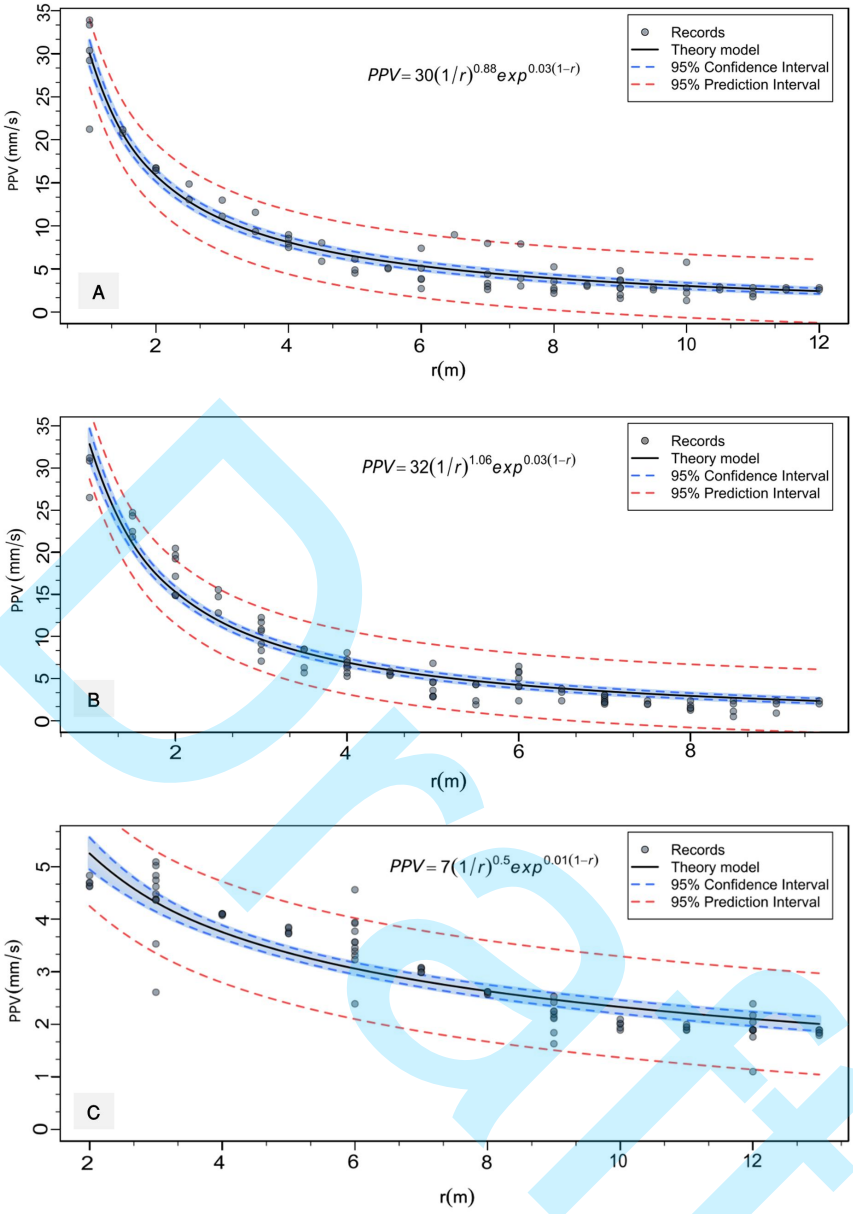

Figure 9: Theoretical model of confidence and prediction (PPV [mm/s] vs. distance r [m]) for the records of the following areas PPV versus r(m): A) Asociación César Vallejo; B) Avenida Cementerio; C) Asociación José Luis Bustamante y Rivero. The turquoise-filled points represent the recorded data, while the black curve indicates the fitted model. The gradient values extending to the blue dashed curve represent confidence intervals up to 95%, and the red dashed lines represent prediction intervals, also up to 95%.

DISCUSSION

Regarding the impact of anthropogenic vibrations, the results obtained for the compaction roller show that this source exceeds all the limit values established by the DIN 4150-3 standard, not only for residential buildings but also for sensitive or historically important structures. In contrast, other anthropogenic sources considered in this study, such as vehicular traffic on bridges and rail transport, have considerably lower vibration levels and therefore represent a much lower potential risk of structural damage. These findings coincide with those of Rodriguez et al. (2022), who emphasized that regulatory limits depend largely on the vulnerability of the structure, with stricter thresholds applying to delicate or historically valuable buildings.

According to Siskind et al. (1980), the **USBM** standard sets particle velocity limits in the frequency range of 3 to 15 Hz, with a maximum of 0.75 inches/second for newer plasterboard homes and 0.50 inches/second for older ones. The results obtained for the roller compactor clearly exceed these values, suggesting that even

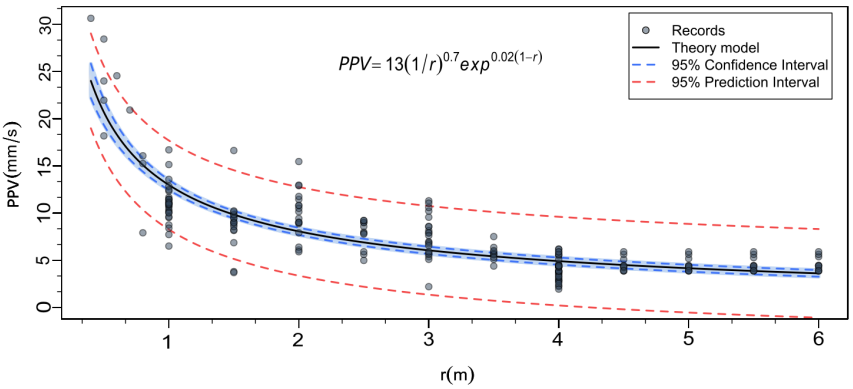

Figure 10: Theoretical model of confidence and prediction (PPV [mm/s] vs. distance r [m]) for the records of the Mansión del Fundador bridge. The turquoise-filled points represent the recorded data, while the black curve indicates the fitted model. The gradient values extending to the blue dashed curve represent confidence intervals up to 95%, and the red dashed lines represent prediction intervals, also up to 95%.

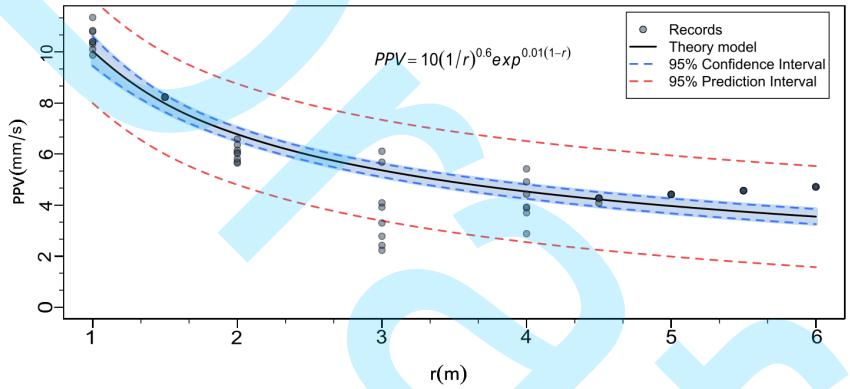

Figure 11: Theoretical model of confidence and prediction (PPV [mm/s] vs. distance r [m]) for the records of the railway transport records on the route from the district of Cerro Colorado to Sachaca. The turquoise-filled points represent the recorded data, while the black curve indicates the fitted model. The gradient values extending to the blue dashed curve represent confidence intervals up to 95%, and the red dashed lines represent prediction intervals, also up to 95%.

relatively resilient residential structures could be at risk. Similarly, British standards (e.g., BS 7385-2 (1993)) set a general limit of 50 mm/s, independent of frequency, for reinforced structures or heavy industrial and commercial buildings. However, for light residential or commercial buildings, the standard specifies decreasing limits in the low frequency range (below 40 Hz), ranging from 20 mm/s at 15 Hz to 15 mm/s at 4 Hz. The values measured in this study for the roller compactor also exceed these thresholds, confirming its role as the source with the greatest potential for structural damage.

In contrast, Spanish standards **UNE 22381-1993 and UNE 22-383** UNE (1993) were not designed to address vibrations generated by machinery or mechanical activities, but rather to regulate those caused by blasting and explosions. These standards are useful in specific contexts, such as mining or controlled demolition, where high-intensity impulsive events predominate. However, they are not appropriate for the assessment of continuous mechanical vibrations produced by heavy machinery, vehicular traffic, or rail transport in urban and industrial environments.

In this regard, the **DIN 4150-3** standard is the most appropriate regulatory framework for assessing anthropogenic vibrations. Its specific focus on vibrations induced by machinery and traffic, its ability to differentiate between structural damage and human comfort, and the definition of thresholds according to the type and sensitivity of buildings ensure an accurate and applicable assessment. Therefore, the adoption of this standard ensures a robust analysis of the risks associated with anthropogenic vibrations and provides a solid basis for the implementation of preventive or corrective measures in case the established limits are exceeded.

Regarding ground vibration attenuation, the results indicate that it is influenced by two primary factors: the expansion of the wavefront (geometric damping) and the dissipation of energy within the ground (material damping). These factors cause the wave amplitude to decrease with distance from the source. It was also observed that in cohesive soils, such as concrete slabs with compact granular material, high porosity, and low humidity, the wave propagation velocity is higher. This reduces stresses in the foundations and minimizes direct transmission to the structure. Conversely, in silty sandy soils with lower porosity and higher humidity, the wave propagation velocity decreases, resulting in increased stress transmitted to the foundations.

To analyze these phenomena, regression adjustment models were developed using the generalized Levenberg-Marquardt inversion method implemented in the RStudio programming language. Neural networks were also applied to automate the analysis of geometric and material damping coefficients. This approach was particularly effective in areas with lower data density, yielding damping coefficient values for γ ranging between (0.1–1.65) and α between (0.001–0.03) for the evaluated sources. The stacked model of vibratory behavior generated by various sources is illustrated in Figures 12a to 12c.

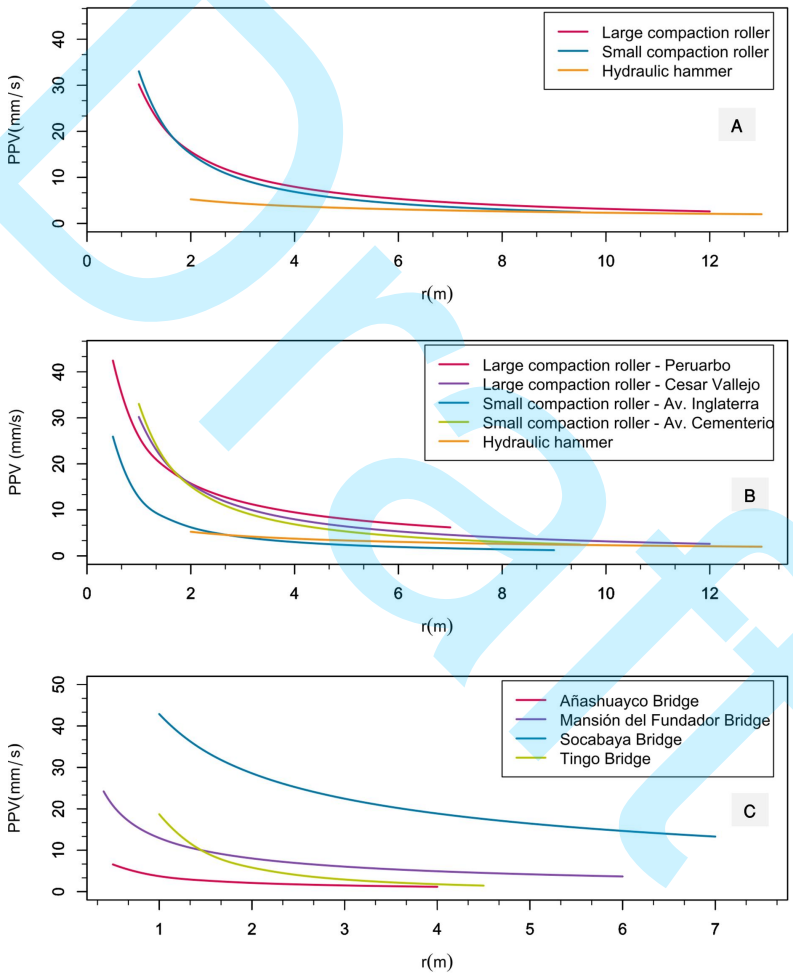

Figure 12: Stacked model of the vibratory behavior generated by various sources: A) A large drum compactor roller at Asociación César Vallejo, a small drum compactor roller on Avenida Cementerio, and an excavator with a hydraulic hammer at Asociación José Luis Bustamante y Rivero; B) Heavy machinery operations; C) Vehicular traffic on bridges.

The values of γ are consistent with those reported according to Kramer (1996) for alluvial soils (0.2–1.5), although the higher values in the study (up to 1.65) for pyroclastic deposits could be attributed to their greater granulometric heterogeneity and porosity, as suggested by Bommer et al. (2000). This variability is explained by the presence of volcanic fragments of varying sizes and degrees of consolidation, which enhance energy dissipation. Conversely, the values of α align with the ranges for cohesive soils (0.005–0.02) reported according to Seed and Idriss (1970), reflecting the capacity of Arequipa's clayey soils to dissipate seismic energy. Furthermore, these results are consistent with BS 7385-2 (1993), which establishes that waves with higher

propagation velocities induce lower vibrations in building foundations. This is consistent with the findings of Chen et al. (2019), who noted that vibration attenuation is faster in coarse-grained soils compared to fine-grained soils. This behavior can be attributed to the high porosity and low moisture content of coarse-grained soils, which results in greater energy loss of vibration waves. Similarly, the findings agree with Auersch and Said (2010), who studied ground vibrations caused by various sources. They analyzed vibration attenuation and propagation characteristics, observing that ground vibration decreases exponentially with distance. Additionally, the results are in line with Toplak et al. (2014), who emphasized the superiority of artificial neural networks and neurofuzzy techniques in predicting vibrations, underscoring the importance of having sufficient experimental data. From the modeled data for different sources and study areas, the damping coefficients exhibited consistent attenuation behavior, corroborating previously published research and reflecting the influence of soil types in the recording regions.

To establish a robust correlation between between soil characteristics and vibratory response, the elevated peak particle velocities (PPV) in compacted soils (>20 mm/s) were analyzed, demonstrating slower attenuation, as evidenced by flatter decay curves and reduced damping coefficients (γ: 0.1–0.5; α: 0.001–0.01). This behavior is attributed to the lower geometric dispersion in dense, compacted soils, which facilitates more efficient vibratory wave propagation, as reported according to Seed and Idriss (1970). These authors indicate that cohesive and compacted soils, owing to their high stiffness, exhibit lower values compared to unconsolidated soils, resulting in limited energy dissipation. Similarly, Dowding (1996) emphasizes that this reduced attenuation in compacted soils increases the stresses transferred to structures, a critical factor for assessing structural risks in seismic regions such as Arequipa.

Although the presented results and models demonstrate robustness and align with established literature, they exhibited limitations, primarily arising from challenges in accessing anthropogenic vibration sources, with railway train access being the most critical, as data acquisition occurred during the COVID-19 pandemic lockdown and amid large-scale regional strikes against mining activities in Arequipa, Peru. This curtailed in-situ measurements and temporal data coverage, aspects that were compensated via the application of neural networks to infer attenuation patterns in data-limited scenarios, thereby preserving the robustness of the predictive modeling. Nevertheless, future investigations are recommended to incorporate additional geophysical assays, facilitating result comparisons and model validation across diverse contexts.

CONCLUSIONS

Analysis of the modeled data across different vibration sources and study areas revealed that the observed damping coefficients align well with previously published research and reflect the expected attenuation behavior based on the soil types in the recording regions. The study was conducted to evaluate the impacts of different urban sources of vibrations and the vulnerability of different structures. The following conclusions are drawn.

Overall, the vibration levels generated by the heavy machinery, vehicular bridge traffic, and railway transport exceed the limits specified by DIN 4150-3 to prevent structural damage. Vibrations from compaction rollers exhibit intermediate frequencies (20–60 Hz) with high peak particle velocities (PPV) ranging from 25–40 mm/s. In contrast, vehicular bridge traffic produces lower frequencies (<20 Hz) with similarly high PPVs (40 mm/s), while railway transport generates intermediate frequencies (30–60 Hz) but lower PPVs (<20 mm/s).

The attenuation of the vertical component of ground vibration amplitude with distance is influenced by two primary factors: geometric and material damping. Consistent with previous studies, local site conditions, such as soil type, have a direct impact on wave propagation. In cohesive soils, as well as in compact granular materials or concrete slabs with high porosity and low moisture content, wave propagation velocities are higher. This reduces the stress transmitted to foundations and the direct impact on structures. Conversely, in silty sandy soils with lower porosity and higher moisture content, wave propagation velocities decrease, leading to increased stress transmission to foundations. The greater the strength of the fill and the stiffness of the soil, the lower the plastic deformation under tensile forces.

It is recommended to establish a specific national regulation to address the effects of anthropogenic vibrations on buildings, as there are currently no technical standards in Peru governing this type of impact. This study can serve as a foundation for future research incorporating additional geophysical techniques, aimed at comparing and validating the developed models, and ultimately contributing to the establishment of a local regulatory framework.

ACKNOWLEDGMENTS

The authors express their gratitude to the Universidad Nacional de San Agustín de Arequipa for financing the project through UNSA INVESTIGA (grant number IBA IB-71-2020-UNSA). GSF is supported by a Research Fellowship grant from CNPq (303199/2025-3).

DATA AND MATERIALS AVAILABILITY

The data used in this research are private.

SUPPLEMENTARY MATERIAL

Table 1: Summary of material and geometric attenuation coefficients reported in the literature

Authors	**Material Type**	**Att. coeff.** $\alpha(m^{-1})$
Forssblad (1965)	Silty gravelly sand	0.131
Richart (1962)	Concrete slab over compact granular fill	0.02
Woods (1967)	Silty fine sand	0.262
Dalmatov et al. (1968)	Sand and silts	0.026 – 0.361
Authors	**Material Type**	**Att. coeff.** γ
Wiss (1967)	Sands	1
	Clays	1.5
Brenner and Chittikuladilok (1975)	Surface sands	1.5
	Sand fill over soft clays	0.8 – 1.0
Attewell and Farmer (1973b)	Various soils, generally firm	1
Nichols et al. (1971)	Firm soils and rock	1.4 – 1.7
Martin (1980)	Clay	1.4
	Silt	0.8
Amick and Ungar (1987)	Clay	1.5

Note. Obtained and adapted from Amick and Gendreau (2000)

Table S2: Vibration data used in accordance with DIN 4150-3, artificial neural networks, and the theoretical regression model employed in this study (see in Excel format).

Figures

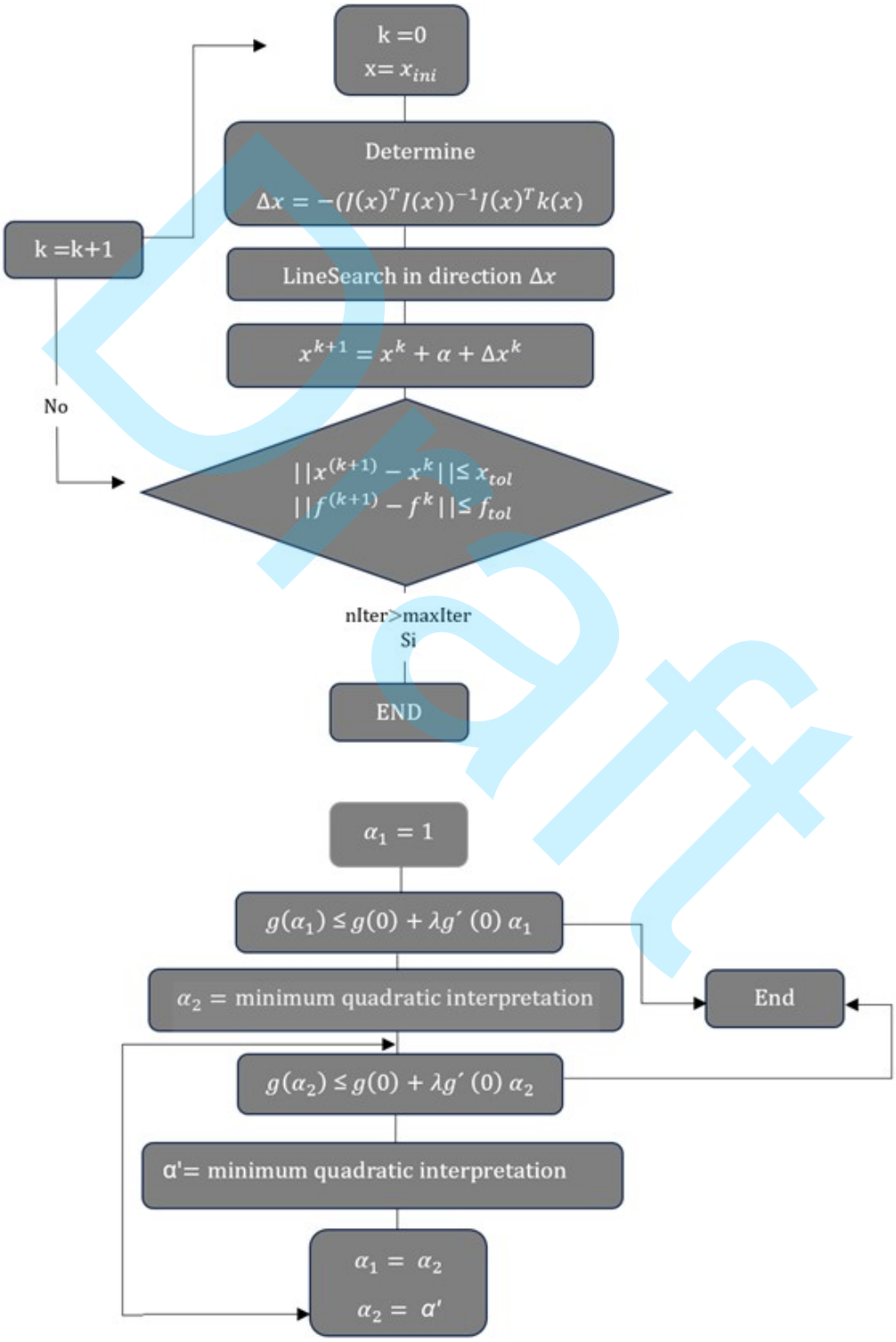

Figure S1: Flowchart of the Levenberg-Marquardt (LM) optimization algorithm.

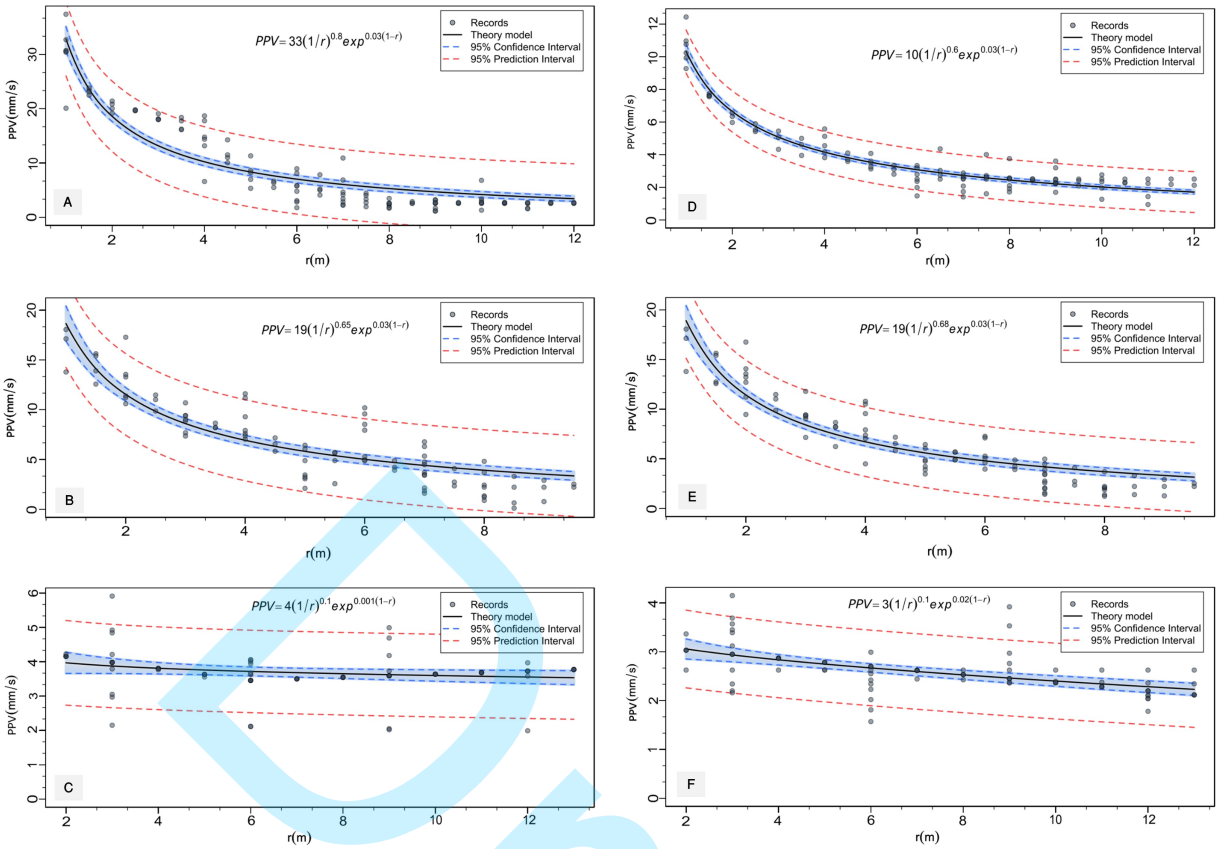

Figure S2: Theoretical model of confidence and prediction for the records obtained in the longitudinal component of the compactor roller (A, B) and an excavator with a hydraulic hammer (C), as well as in the transversal component of the compactor roller (D, E) and an excavator with a hydraulic hammer (F). These measurements were conducted in Asociación César Vallejo, Avenida Cementerio, and José Luis Bustamante y Rivero, respectively.

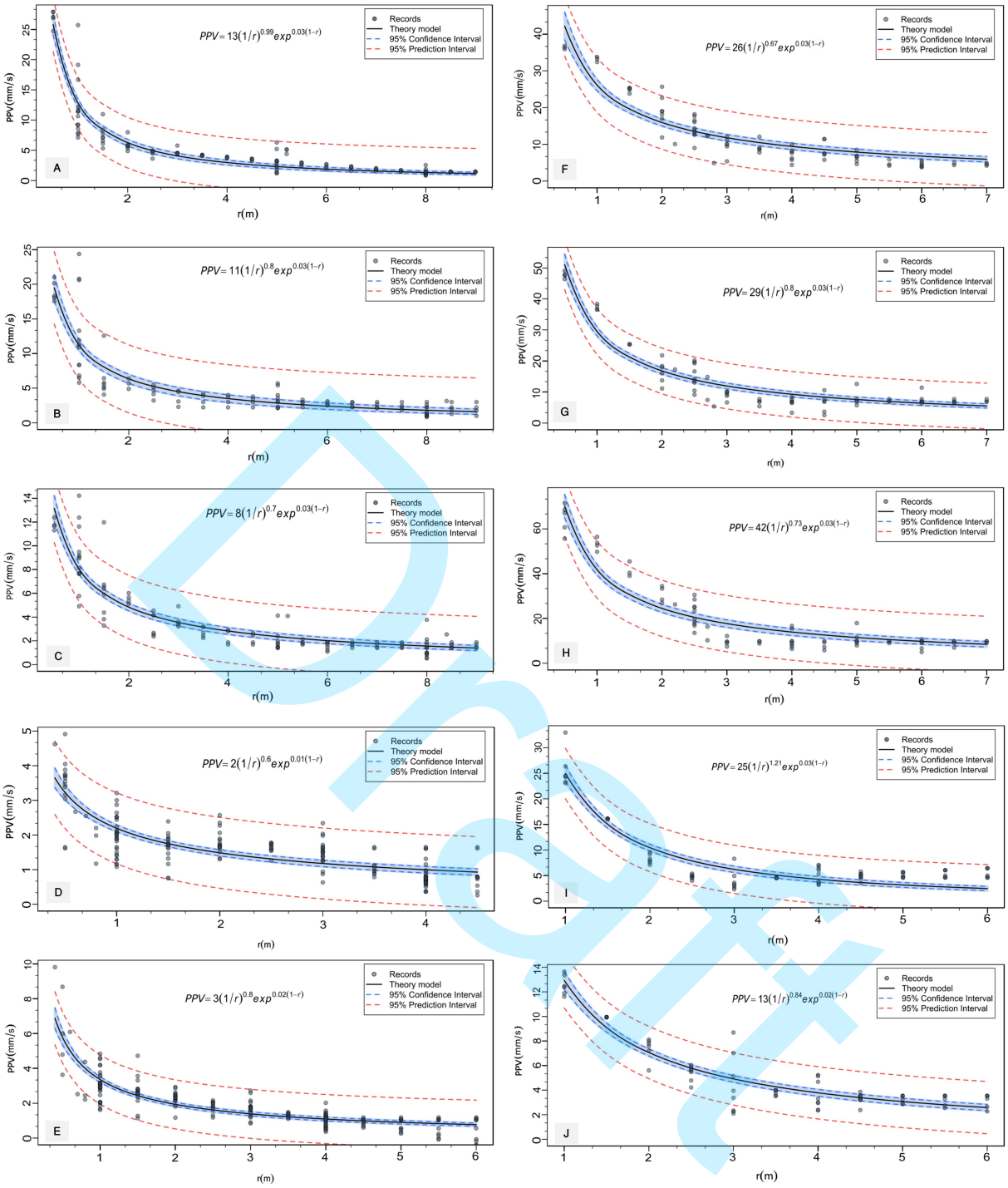

Figure S3: Theoretical model of confidence and prediction for the records obtained from various vibration sources. Heavy machinery (large drum compactor roller) was analyzed on Avenida Inglaterra (A, B, C) and in the Peruarbo Asociación (F, G, H), considering its three components: vertical, longitudinal, and transversal. Vehicular circulation on the Mansión del Fundador bridge was evaluated in its longitudinal and transversal components (D, E). Lastly, railway transport on the route from the district of Cerro Colorado to Sachaca was analyzed in its longitudinal and transversal components (I, J).

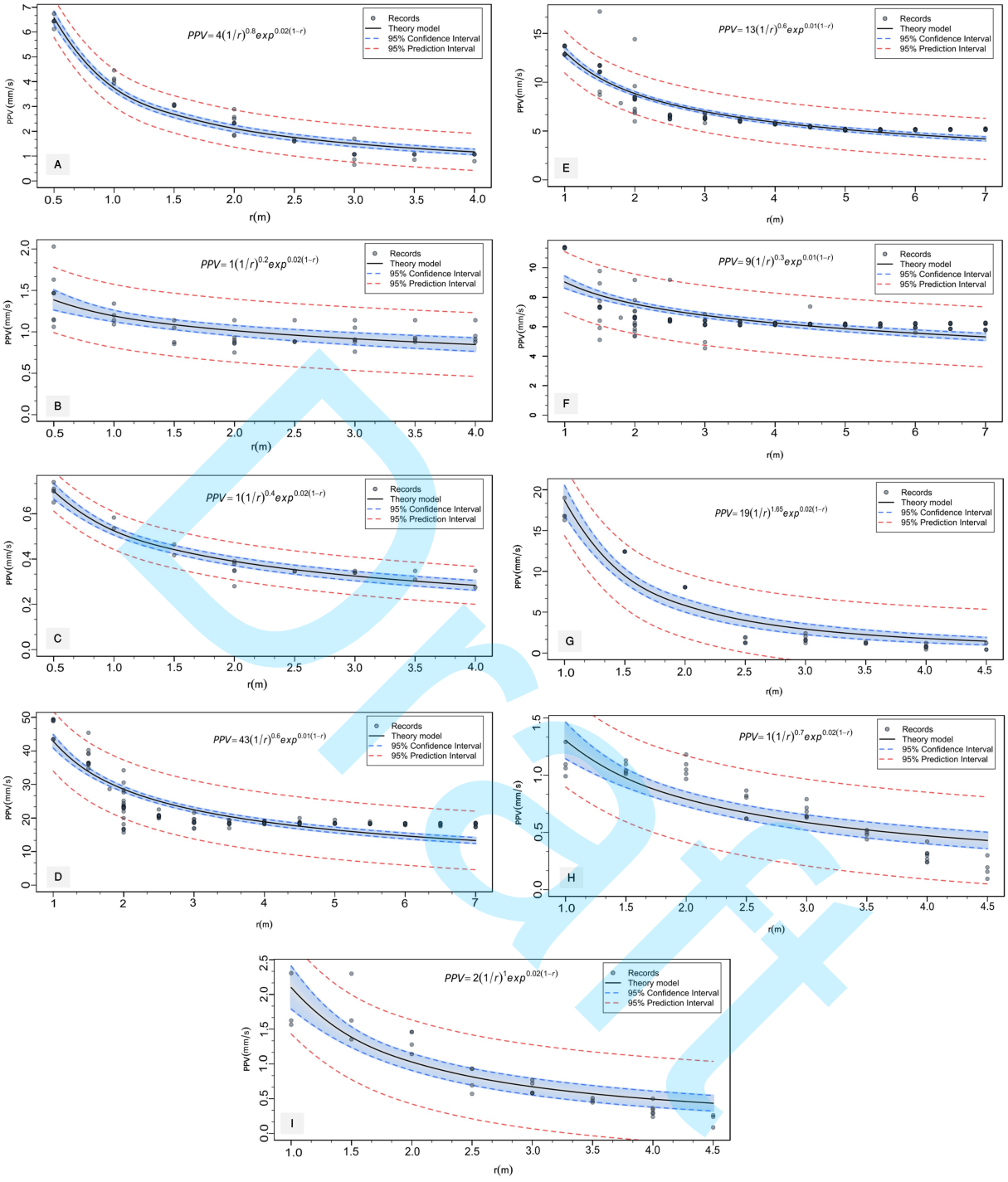

Figure S4: Theoretical model of confidence and prediction for the records obtained from vehicular traffic on three bridges. The Añashuayco Bridge was analyzed in its vertical, longitudinal, and transversal components (A, B, C), followed by the Socabaya Bridge (D, E, F) and the Tingo Bridge (G, H, I), each evaluated across the same three components.

AUTHOR CONTRIBUTIONS

1st Author: Data acquisition, analysis and processing of the data, figure editing and writing the manuscript; **2nd Author**: Data acquisition, analysis and processing of the data, figure editing and writing the manuscript; **3rd Author**: Data acquisition, analysis and processing of the data; **4th Author**: Participation as advisor in the processing of data and discussion of results, and revision of the manuscript; **5th Author**: Data acquisition; **6th Author**: Contributed to the design and implementation of the research, to the analysis of the results, and the writing of the manuscript; **7th Author**: Data acquisition; **8th Author**: Participation as advisor in the processing of data and discussion of results, and revision of the manuscript.

CONFLICTS OF INTEREST

The authors declare no conflict of interest.

COPYRIGHT AND OPEN ACCESS

REFERENCES

Abadi, M., P. Barham, J. Chen, Z. Chen, A. Davis, J. Dean, M. Devin, S. Ghemawat, G. Irving, M. Isard, et al., 2016, Tensorflow: Large-scale machine learning on heterogeneous distributed systems: https://www.tensorflow.org/.

Adam, D., C. Adam, F.-J. Falkner, and I. Paulmichl, 2011, Vibration emission induced by rapid impact compaction: Proceedings of 8th International Conference on Structural Dynamics, EURODYN 2011, G. De Roeck, G. Degrande, G. Lombaert, G. M¨uller, 914–921. url: https://www.researchgate.net/publication/314044572_Vibration_emission_induced_by_Rapid_Impact_Compaction.

Aguilar, Z., and J. Alva, 1991, Microzonificacion sismica de la ciudad de arequipa: Presented at the Presentation at the VI National Congress of Soil Mechanics and Foundation Engineering, Lima, Peru. url: https://www.jorgealvahurtado.com/files/redacis19_a.pdf.

Amick, H., 1999, A frequency-dependent soil propagation model: Presented at the , Proceedings of the International Society for Optical Engineering (SPIE), Vol. 3786, Denver CO, USA. url: https://colingordon.com/research/a-frequency-dependent-soil-propagation-model/.

Amick, H., and M. Gendreau, 2000, Construction vibrations and their impact on vibration-sensitive facilities: Presented at the Proceedings of the ASCE Construction Congress VI, American Society of Civil Engineers.

Amick, H., and E. E. Ungar, 1987, Evaluation of ground and structural vibrations from pile driving: Technical Report BBN Report No. 6427, Bolt, Beranek and Newman Inc.

Athanasopoulos, G., and P. Pelekis, 2000, Ground vibrations from sheetpile driving in urban environment: measurements, analysis and effects on buildings and occupants: Soil Dynamics and Earthquake Engineering, **19**, no. 5, 371–387, doi: 10.1016/S0267-7261(00)00008-7.

Attewell, P. B., and I. W. Farmer, 1973a, Attenuation of ground vibrations from pile driving: Ground engineering, **6**, no. 7, 26–29.

Attewell, P. B., and I. W. Farmer, 1973b, Attenuation of ground vibrations from pile driving: Ground Engineering, **3**, 26–29.

Auersch, L., 2010, Technically Induced Surface Wave Fields, Part I: Measured Attenuation and Theoretical Amplitude-Distance Laws: Bulletin of the Seismological Society of America, **100**, no. 4, 1528–1539, doi: 10.1785/0120090228.

Auersch, L., and S. Said, 2010, Attenuation of ground vibrations due to different technical sources: Earthquake Engineering and Engineering Vibration, **9**, no. 3, 337–344, doi: 10.1007/s11803-010-0018-0.

Bishop, C. M., 1995, Neural networks for pattern recognition: Oxford University Press.

Bommer, J. J., N. N. Ambraseys, and S. K. Sarma, 2000, The attenuation of ground accelerations in europe: a revision: Bulletin of the Seismological Society of America, **90**, 1193–1204.

Brenner, R. P., and B. Chittikuladilok, 1975, Vibrations from pile driving in the bangkok area: Geotechnical Engineering, **5**, 167–197.

BS 7385-2, 1993, Evaluation and measurement for vibration in buildings – part 2: Guide to damage levels from ground-borne vibration: Technical Report BS 7385-2, British Standards Institution, London, UK.

Burgemeister, K., K. Fisher, and K. Franklin, 2011, Measurement and prediction of construction vibration affecting sensitive laboratories: Conference: Proc. Acoustics 2011, At: Gold Coast, 20–26. url: https://www.acoustics.asn.au/conference_proceedings/AAS2011/papers/p33.pdf.

Chen, A., F. Cheng, D. Wu, and X. Tang, 2019, Ground vibration propagation and attenuation of vibrating compaction: Journal of Vibroengineering, **21**, no. 5, 1342–1352, doi: 10.21595/jve.2019.20388.

Chollet, F., et al., 2015, Keras: https://keras.io.

Coleman, T., and A. Verma, 2001, A preconditioned conjugate gradient approach to linear equality constrained minimization: Computational Optimization and Applications, **20**, no. 1, 61–72, doi: 10.1023/A:1011271406353.

Costa, P., 2011, Vibrações do sistema via-maciço induzidas por tráfego ferroviário : modelação numérica e validação experimental: Presented at the . url: https://api.semanticscholar.org/CorpusID:176382213.

Dalmatov, B. I., V. A. Ershov, and E. D. Kovalevsky, 1968, Some cases of foundation settlement in driving sheeting and piles: Proceedings of the International Symposium on Wave Properties of Earth Materials, 607–613.

Del Castillo Martinez, I., 2012, Control of vibrations generated by the passage of two tunnel boring machines under the buildings in the urban area of vigo: Ingeopres: Technical news on civil engineering, mining, geology and the environment, 22–25.

DIN 4150-3, 1993, Vibrations in buildings – part 3: Effects on structures: Technical report, Deutsches Institut für Normung e.V.

Dowding, C. H., 1996, Construction vibrations: Prentice Hall.

Dowding, K., J.-E. Lane, and N. R. Miller, 1996, Journal of theoretical politics: Sage Publications, **8**, no. 1, 5–6, doi: 10.1177/0951692896008001001.

Ekanayake, S., D. Liyanapathirana, and C. Leo, 2013, Influence zone around a closed-ended pile during vibratory driving: Soil Dynamics and Earthquake Engineering, **53**, 26–36, doi: 10.1016/j.soildyn.2013.06.005.

Forssblad, L., 1965, Investigations of soil compaction by vibration: Technical Report 34, Royal Swedish Academy of Engineering Sciences.

Gasmi, H., K. Ben Abdallah, E. Hamdi, B. Achour, T. Butt, and N. Ghazouani, 2023, Combined blast and vibratory machines effect on in-service structures: Alexandria Engineering Journal, **64**, 591–600, doi: 10.1016/j.aej.2022.09.014.

Glorot, X., A. Bordes, and Y. Bengio, 2011, Deep sparse rectifier neural networks: Proceedings of the Fourteenth International Conference on Artificial Intelligence and Statistics, PMLR, 315–323. url: http://proceedings.mlr.press/v15/glorot11a.html.

Goodfellow, I., Y. Bengio, and A. Courville, 2016, Deep learning: MIT Press.

Hegde, A., and H. Venkateswarlu, 2019, Mitigation of Traffic Induced Vibration Using Geocell Inclusions: Frontiers in Built Environment, **5**, doi: 10.3389/fbuil.2019.00136.

IGP, 2017, Peligros geodinámicos en la ciudad de arequipa cercado y zonas aledañas: Technical report, Instituto Geofísico del Perú (IGP), `https://sinia.minam.gob.pe/sites/default/files/sinia/archivos/public/docs/informe_tecnico_peligros_geodinamicos_en_arequipa.pdf`.

INEI, 2018, Características de las viviendas particulares y los hogares: Technical report, Instituto Nacional de Estadística e Informática, `https://www.inei.gob.pe/media/MenuRecursivo/publicaciones_digitales/Est/Lib1538/Libro.pdf`.

INGEMMET, 2022, Evaluación de peligro geológico por lahares (huaycos) en el distrito de cerro colorado: Technical report, Instituto Geológico, Minero y Metalúrgico del Perú, `https://repositorio.ingemmet.gob.pe/handle/20.500.12544/4308`.

INGEMMET, s.f., Geocatmin: Plataforma de información geológica, minera y catastral del perú: Technical report, Instituto Geológico, Minero y Metalúrgico, https://geocatmin.ingemmet.gob.pe/geocatmin/.

Jiang, Y., F. Meng, Y. Chen, Y. Zheng, X. Chen, J. Zhang, and X. Huang, 2020, Vibration attenuation analysis of periodic underground barriers using complex band diagrams: Computers and Geotechnics, **128**, 103821, doi: 10.1016/j.compgeo.2020.103821.

Khandelwal, M., 2012, Application of an Expert System for the Assessment of Blast Vibration: Geotechnical and Geological Engineering, **30**, no. 1, 205–217, doi: 10.1007/s10706-011-9463-4.

Kingma, D. P., and J. Ba, 2014, Adam: A method for stochastic optimization: arXiv preprint arXiv:1412.6980.

Kramer, S. L., 1996, Geotechnical earthquake engineering: Prentice Hall.

Martin, D. J., 1980, Ground vibrations from impact pile driving during road construction: Technical Report Supplementary Report 554, Transport and Road Research Laboratory.

Mia, M. M., and S. Dhar, 2016, Prediction of blast-induced vibration using artificial neural network: A case study from nirmali open cast coal mine, india: International Journal of Mining Science and Technology, **26**, 773–780, doi: 10.1016/j.ijmst.2016.06.003.

MTC, 2016, Manual ensayo de materiales. Ministerio de Transportes y Comunicaciones - Perú, `https://portal.mtc.gob.pe/transportes/caminos/normas_carreteras/documentos/manuales/Manual%20Ensayo%20de%20Materiales.pdf`.

Nichols, H. R., C. F. Johnson, and W. I. Duvall, 1971, Blasting effects and their effects on structures: Technical

Report Bulletin 656, U.S. Bureau of Mines.
Niu, D., Y. Deng, H. Mu, J. Chang, Y. Xuan, and G. Cao, 2022, Attenuation and propagation characteristics of railway load-induced vibration in a loess area: Transportation Geotechnics, **37**, 100858, doi: 10.1016/j.trgeo.2022.100858.
Ositran, 2017, Informe de desempeño 2017 - concesión del ferrocarril del sur y sur oriente: Technical report, Organismo Supervisor de la Inversión en Infraestructura de Transporte de Uso Público, https://www.ositran.gob.pe/anterior/wp-content/uploads/2017/12/id-2019-fetransa.pdf.
Pistrol, J., F. Kopf, D. Adam, S. Villwock, and W. Völkel, 2013, Ambient vibration of oscillating and vibrating rollers: Presented at the , Proceedings - Vienna Congress on Recent Advances in Earthquake Engineering and Structural Dynamics 2013 (VEESD 2013). url: https://api.semanticscholar.org/CorpusID:13134636.
PMUS, 2022, Plan de movilidad urbana sostenible de arequipa 2022-2042: Technical report, Plan de Movilidad Urbana Sostenible de Arequipa, Mobilise Your City, https://www.mobiliseyourcity.net/sites/default/files/2024-04/2022-10-23_Documento_PMUS-AQP_VFinal%28Word97%29.pdf.
Puzzilli, L. M., G. Bongiovanni, P. Clemente, V. Di Fiore, and V. Verrubbi, 2021, Effects of anthropic and ambient vibrations on archaeological sites: The case of the circus maximus in rome: Geosciences, **11**, no. 11, doi: 10.3390/geosciences11110463.
Rangel, J., 2018, Alternativas para mitigar excesivas vibraciones en puentes peatonales: Master's thesis, Universidad Autónoma de Nuevo León, http://eprints.uanl.mx/id/eprint/15914.
Richart, F. E., 1962, Foundation vibrations: Transactions of the American Society of Civil Engineers, **127**, 863–898.
Rodríguez, R., and M. Bascompta, 2020, Vibration Analysis and Empirical Law Definition for Different Equipment in a Civil Construction: Applied Sciences, **10**, no. 14, 4689, doi: 10.3390/app10144689.
Rodriguez, R., M. Bascompta, P. Fernandez, and P. R. Fernandez, 2022, Representative-area approach to define blast-induced ground vibrations—damage prevention criterion abacus: Minerals, **12**, no. 6, 691, doi: 10.3390/min12060691.
Saucedo, H., 2014, Diseño y aplicación de riego por gravedad: Technical report, Instituto Mexicano de Tecnología del Agua, http://repositorio.imta.mx/bitstream/handle/20.500.12013/1366/RD-1403.1.pdf?sequence=1&isAllowed=y.
Seed, H. B., and I. M. Idriss, 1970, Soil moduli and damping factors for dynamic response analyses: Technical Report EERC 70-10, Earthquake Engineering Research Center, University of California, Berkeley, CA.
Siskind, D. E., M. S. Stagg, J. W. Kopp, and C. H. Dowding, 1980, Structure response and damage produced by ground vibration from surface mine blasting: Technical Report RI 8507, United States Bureau of Mines.
Toplak, S., A. Ivanic, P. Jelusic, and S. Lubej, 2014, Measurement, prediction and modeling the impact of vibration as the possibility of protection cultural heritage objects: International Journal of Physical Sciences Full Length Research Paper, **9**, no. 22, 495–505, doi: 10.5897/IJPS2014.4192.
UNE, 1993, Control de vibraciones producidas por voladuras: Technical report, Asociación Española de Normalización (UNE).
Wiss, J. F., 1967, Damage effects of pile driving vibration: Highway Research Record, 14–20.
Woods, R. D., 1967, Screening of elastic waves by trenches: Journal of the Soil Mechanics and Foundations Division, ASCE, **94**, 951–979.
Yao, J., R. Zhao, N. Zhang, and D. Yang, 2019, Vibration isolation effect study of in-filled trench barriers to train-induced environmental vibrations: Soil Dynamics and Earthquake Engineering, **125**, 105741, doi: 10.1016/j.soildyn.2019.105741.

Received on / Accepted on